11 Instrumentation and Methodology

11-1 X-Ray Phase-Contrast Imaging Using an X-Ray HARP Camera

When X-rays propagate through an object, their wave front is deformed due to phase shifts caused by the object. X-ray phase-contrast imaging detects these phase shifts to observe the inner structures of various objects non-destructively. Since sensitivity is much higher than that of conventional absorption-contrast imaging methods, many studies have been made of this innovative imaging technique. Among others, X-ray interferometry [1] and X-ray angle-resolved imaging [2] have been intensively pursued at the Photon Factory.

To date, area detectors such as X-ray films, imaging plates and X-ray CCD cameras have been widely used for phase-contrast imaging. However, to further improve the performance of the overall imaging system requires the development of an X-ray area detector with higher sensitivity and better spatial resolution. One of the most promising candidates satisfying these requirements is an X-ray HARP camera [3]. The HARP camera is an image pick-up tube with an amorphous selenium (a-Se) photoconductive target and is characterized by its internal amplification process. The process uses an avalanche phenomenon in the photoconductive layer. We have successfully applied an X-ray HARP camera to X-ray phase-contrast imaging for the first time.

The experimental setup at BL-14B is schematically shown in Fig. 1. A monochromatic X-ray beam of energy 16.2 keV was generated using a Si(111) double-crystal monochromator. The beam was collimated and expanded using an asymmetric Si(220) collimator crystal, and passed through a sample. The refraction angle of the X-rays transmitted through the sample is given by

$$\alpha_x(x, y) \approx \frac{1}{k}\frac{\partial \phi(x, y)}{\partial x}, \quad \alpha_y(x, y) \approx \frac{1}{k}\frac{\partial \phi(x, y)}{\partial y},$$

where $\phi(x, y)$ is the phase shift due to the sample, k is the wavenumber, and the z-axis is parallel to the propagation direction of the X-rays. The refraction angle, $\alpha_y(x, y)$, was measured using a symmetric Si(220) analyzer crystal and the X-ray HARP camera. The pixel size of the camera was 8 μm × 15 μm. A voltage of 1300 V was applied to the 15-μm-thick a-Se layer. The frame rate was 30 fps and 30 images were accumulated for analysis. Figure 2 shows images obtained from a rat liver sample. The field of view is 400 pixels × 400 pixels. Al-

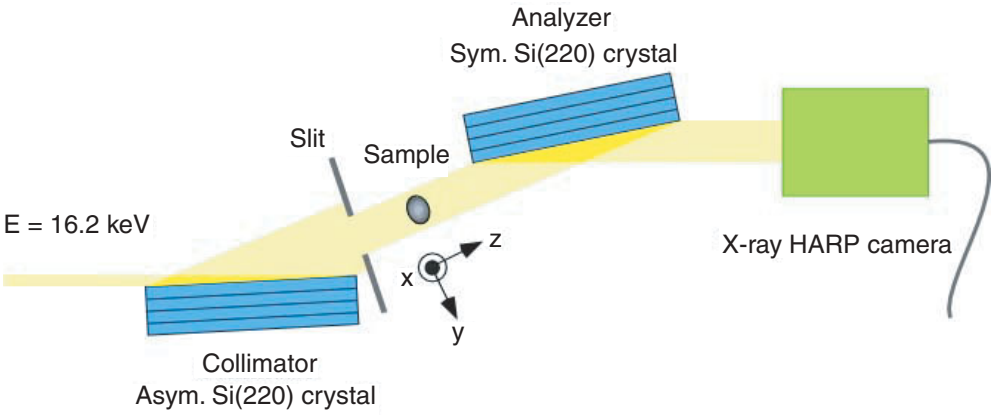

Figure 1
Experimental setup for angle-resolved X-ray imaging using an X-ray HARP camera.

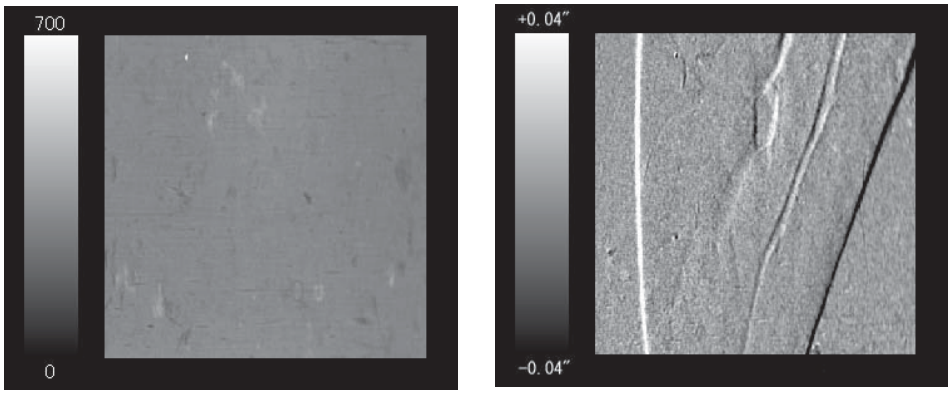

Figure 2
Projection images of a rat liver. (a) Absorption contrast. (b) Phase contrast.

though no structure is visible in the absorption-contrast image shown in Fig. 2(a), shape and internal structures such as those of blood vessels are clearly seen in the phase-contrast image of Fig. 2(b). The refraction angle of the X-rays transmitted through the sample was found to be distributed between –0.04" and +0.04". The sensitivity of the X-ray HARP camera has been shown to be higher than that of a fiber-coupled X-ray CCD camera. This result indicates that the X-ray HARP camera is very useful for the X-ray phase-contrast imaging.

The experiment was approved by the Medical Committee for the use of animals in research of the University of Tsukuba and KEK.

K. Hirano[1], T. Miyoshi[1], N. Igarashi[1], T. Takeda[2], J. Wu[2], T. T. Lwin[2], M. Kubota[3], N. Egami[3], K. Tanioka[3], T. Kawai[4] and S. Wakatsuki[1] ([1]KEK-PF, [2]Tsukuba Univ., [3]NHK, [4]NHK-ES)

References

[1] A. Momose, T. Takeda, Y. Itai and K. Hirano, *Nature Medicine*, **2** (1996) 473.
[2] K. Hirano, *J. Phys. D,* **36** (2003) 1469.
[3] K. Tanioka and T. Hirai, *OYO BUTURI,* **71** (2002) 1376.

11-2 Nonreciprocal Magnetoelectric X-Ray Scattering in Magnetite Fe_3O_4

In magnetically ordered crystals where time reversal *R* and space inversion *I* symmetries are broken simultaneously, unique nonreciprocal magneto-optical phenomena, termed magnetochiral or X-ray magnetoelectric (ME) effects, are expected to show up as characterized by different X-ray response (absorption or refraction) depending on X-ray propagation direction *k* [1,2]. A spectroscopic study of this nonreciprocal ME effect is important to clarify the microscopic mechanism of the ME effect which is attracting renewed interest also from the viewpoint of applications to spintronics.

However, the appearance of such an effect is limited to rather exceptional materials in which *R* and *I* symmetries are both broken. Such a limitation can be circumvented by using anomalous X-ray scattering [3,4]. ME X-ray scattering (MEXS) enables us to detect the local ME effect at noncentrosymmetric site, even in systems where *I* symmetry is globally restored. We have adopted spinel-type ferrimagnet Fe_3O_4 as a good candidate for the ME X-ray scattering spectroscopy. It has a centrosymmetric structure at room temperature. While the octahedral B sites (O_h) have an inversion center, *I* symmetry is locally broken at the tetrahedral A sites (T_d).

The measurements of magnetic (magnetoelectric) X-ray scattering were carried out on BL-1A. An X-ray beam was incident onto an Fe_3O_4(111) surface. A modulated magnetic field with an amplitude of H = 800 Oe was applied along the direction perpendicular to the scattering plane, namely in Voigt configuration. The magnetic and/or ME scattering intensity was recorded as the ratio of spin-dependent to spin-independent scattering intensity $\Delta I / I$.

Figure 3(a) shows an X-ray absorption spectrum of Fe_3O_4 powder at room temperature in the vicinity of the Fe K-absorption edge. A weak absorption at 7.117 keV can be assigned to the Fe 1*s* → Fe 3*d* transition (pre-edge) occurring mainly at the noncentrosymmetric A sites, whereas the second strong peak (~ 7.134 keV) is attributed to the Fe 1*s* → Fe 4*p* transition (main edge) at both the A and B sites. Figure 3(b) shows the magnetic X-ray scattering spectra at the (222), (333), (444) Bragg reflections. Taking into consideration that the ME scattering factor changes the sign not only by *R* but also by *I* operation, the ME scattering signal is expected to be maximized at the (222) reflection. From the structure factor analysis, we have confirmed that the resonant enhancement of $\Delta I / I$ as large as 1% observed around the pre-edge at the (222) reflection is ascribed to MEXS. In the inset of Fig. 4, we show the temperature dependence of magnetic (mostly ME) X-ray scattering spectra at the (222) reflection. The temperature variation of $\Delta I / I$ at the peak energy (~ 7.116 keV) is similar to that of magnetization curve in a field of 800 Oe.

These results suggest a possibility that the present element-specific resonant MEXS spectroscopy may be applied to a broad class of magnetic materials with noncentrosymmetric magnetic sites, including magnetic superlattices, interfaces and junctions [5].

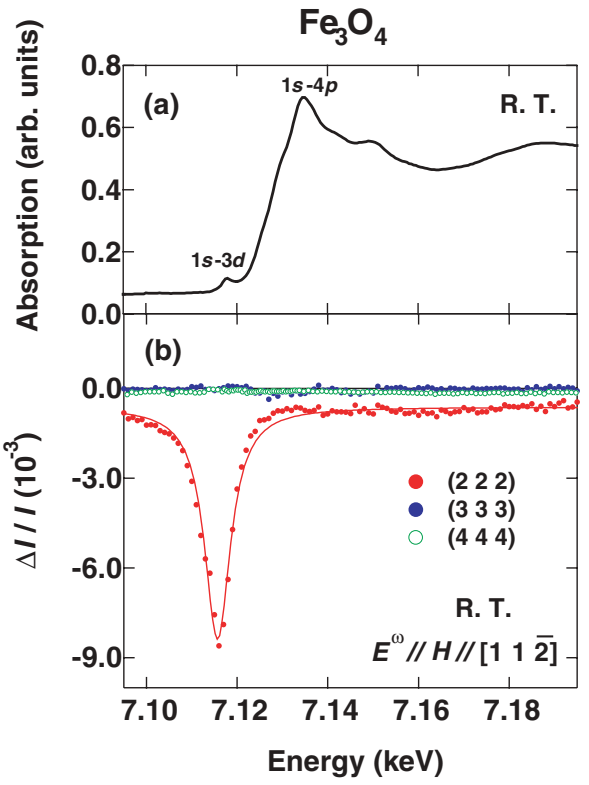

Figure 3
(a) Absorption spectrum of pulverized crystal and (b) magnetic (including magnetoelectric) scattering spectra $\Delta I / I$ at the (222) (red), (333) (blue), (444) (green) reflections at room temperature in the vicinity of the Fe K-absorption edge in Fe_3O_4 crystal.

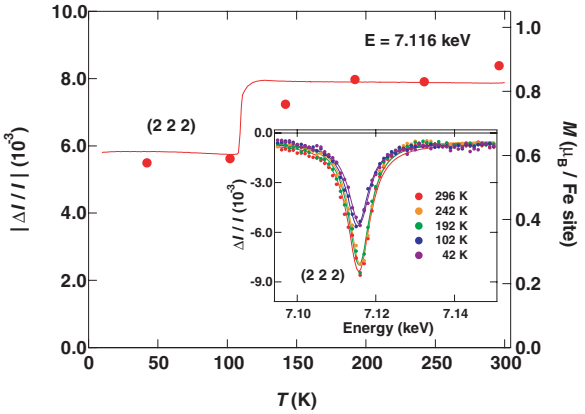

Figure 4
The variation of magnetic scattering intensity $\Delta I / I$ at the peak energy (~ 7.116 keV) at the (222) reflection. The inset shows the temperature dependence of magnetic (mainly magnetoelectric) scattering spectra.

M. Matsubara[1], Y. Shimada[2], T. Arima[3], Y. Taguchi[3] and Y. Tokura[1,2] ([1]AIST, [2]The Univ. of Tokyo, [3]Tohoku Univ.)

References

[1] J. H. Jung, M. Matsubara, T. Arima, J. P. He, Y. Kaneko and Y. Tokura, *Phys. Rev. Lett.*, **93** (2004) 037403.
[2] M. Kubota, T. Arima, Y. Kaneko, J. P. He, X. Z. Yu and Y. Tokura, *Phys. Rev. Lett.*, **92** (2004) 137401.
[3] S. Di Matteo, Y. Joly, A. Bombardi, L. Paolasini, F. de Bergevin and C. R. Natoli, *Phys. Rev. Lett.*, **91** (2003) 257402.
[4] T. Arima, J. H. Jung, M. Matsubara, M. Kubota, J. P. He, Y. Kaneko and Y. Tokura, *J. Phys. Soc. Jpn.*, **74** (2005) 1419.
[5] M. Matsubara, Y. Shimada, T. Arima, Y. Taguchi and Y. Tokura, *Phys. Rev. B*, **72** (2005) 220404 (R).

11-3 Development of a Scanning Tunneling Microscope for Elemental Analysis Using Synchrotron Radiation

Scanning tunneling microcopy (STM) provides us with information on the atomic-scale structure of sample surfaces with high spatial resolution. It is, however, not easy to obtain chemical or elemental information using STM except for a few special cases such as inelastic electron-tunneling spectroscopy, which is sensitive to the vibrational energies of individual adsorbed molecules. The reason for the difficulty in general is simply because STM probes the tunneling current, which basically reflects the valence electronic states of the sample. To access elemental information requires the probing of core-level electrons, in a similar manner to Auger and X-ray photoelectron spectroscopy. In this project, we have constructed an ultrahigh vacuum (UHV) STM in which core-level electrons are excited by an irradiation of a sample with synchrotron radiation (SR), and the resulting photo-induced currents are detected by an STM probe tip (SR-STM) (Fig. 5) [1,2]. In addition to high intensity, a further advantage of using SR is that the photon energy can be tuned so that core electrons of a specific element are excited, allowing us to make an elemental analysis.

The performance of the system was tested using a standard Si(111)-7×7 surface sample. All experiments were carried out at BL-19A. Despite mechanically and electronically noisy conditions, atomically-resolved images of the surface were successfully obtained, demonstrating the stability of the UHV-STM system. The detection of photo-induced electrons with the tip was tested by generating STM images of the Si surface under SR illumination with various photon energies ranging from 96 eV to 106 eV, spanning the Si 2*p* absorption edge at 99 eV. When photo-induced electrons are detected by the tip, the tip is retracted from the surface by the STM feedback system as it tries to keep the total current constant. Consequently the image appears bright (high) when extra current is detected (Fig. 6). We found a sharp increase in height at the Si absorption-edge energy, indicating the possibility of recording X-ray absorption spectra using the STM tip in the tunneling regime.

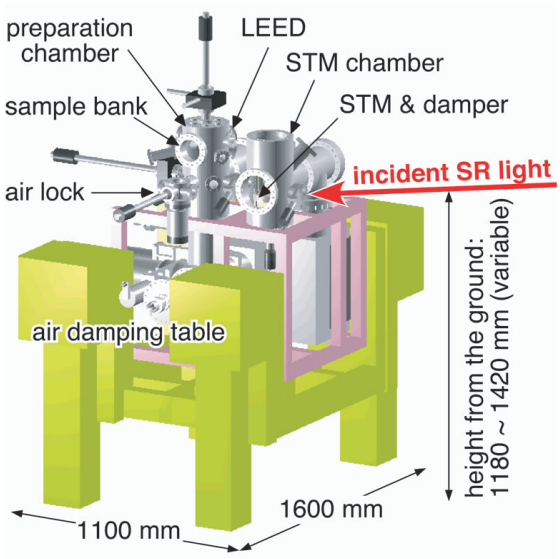

Figure 5
Schematic of the SR-STM system

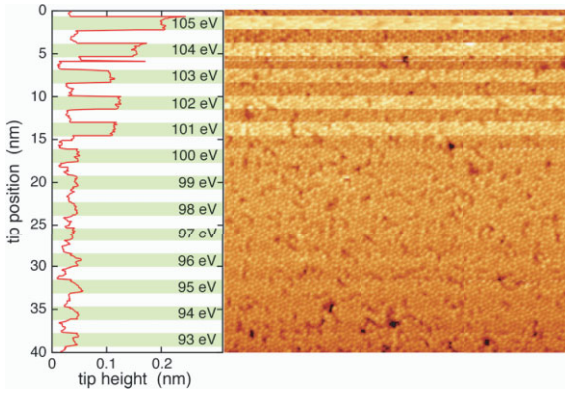

Figure 6
STM image (right) of a Si(111)7×7 surface. The image was generated by scanning the energy of the incident synchrotron radiation from 93 eV (bottom line of the image) to 105 eV (top line of the image). The average height at each horizontal line of the image is plotted in the panel on the left.

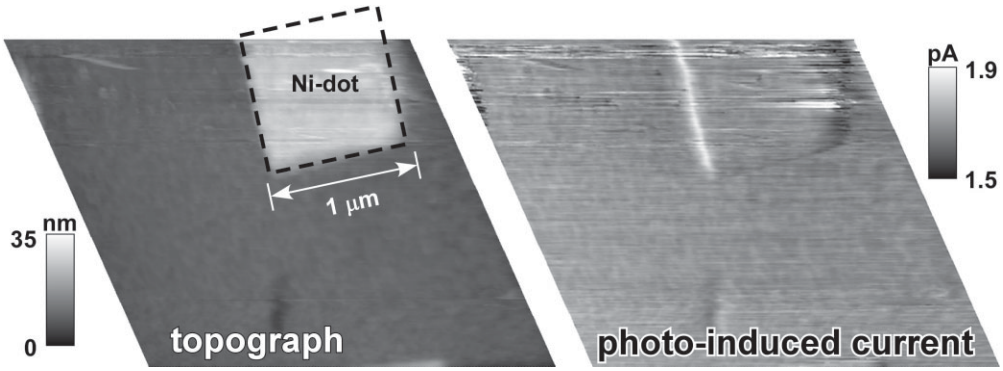

Figure 7
Topographic STM image of Ni dots fabricated on a thin Au film (left), and the simultaneously obtained photo-induced current image (right). The images were generated by irradiation of the sample with SR with a photon energy of 855 eV, slightly above the Ni L_3 edge at 852.7 eV.

In order to confine the probed area in the above-mentioned XAS-with-STM-tip method, we developed a glass-coated tip for blocking electrons coming from the tip side [3]. To prepare the tip, it was first completely covered with glass and repeatedly heated until the thickness of the glass layer became thinner than 10 μm. The thin glass on the tip apex was then removed using a focused ion beam (FIB). The uncovered area was less than 5 μm from the tip apex. This glass-coated tip was found to be quite effective for the reduction of undesired background current. In the XAS measurement, the background was reduced by a factor of 40. Using the tip made it possible to measure the photo-induced current on a sample consisting of 1-μm-square Ni dots on a Au-coated Si(001) wafer at BL-13C. It allowed us also to observe an enhancement of the photo-induced current from the Ni dots when the incident photon energy (855 eV) is just above the Ni absorption edge. The photo-induced current images recorded with the same photon energy clearly resolve the location of the Ni dots (Fig. 7) [4], demonstrating the possibility of element-specific imaging using this technique.

T. Eguchi, T. Okuda, T. Matsushima, A. Kataoka, A. Harasawa, K. Akiyama, T. Kinoshita and Y. Hasegawa (The Univ. of Tokyo)

References

[1] T. Matsushima, T. Okuda, T. Eguchi, M. Ono, A. Harasawa, T. Wakita, A. Kataoka, M. Hamada, A. Kamoshida, Y. Hasegawa and T. Kinoshita, *Rev. Sci. Instrum.*, **75** (2004) 2149.
[2] T. Okuda, T. Eguchi, T. Matsushima, M. Hamada, X. -D. Ma, A. Kataoka, A. Harasawa, T. Kinoshita and Y. Hasegawa, *J. Electron Spectrosc. Relat. Phenom.*, **144-147C** (2005) 1157.
[3] K. Akiyama, T. Eguchi, T. An, Y. Hasegawa, T. Okuda, A. Harasawa and T. Kinoshita, *Rev. Sci. Instrum.*, **76** (2005) 083711.
[4] T. Eguchi, T. Okuda, T. Matsushima, A. Kataoka, A. Harasawa, K. Akiyama, T. Kinoshita and Y. Hasegawa, *Appl. Phys. Lett.*, to be published.